Giant magnetoresistance in zigzag graphene nanoribbon

Z. F. Wang and Feng Liu

Related Articles

Additional information on Appl. Phys. Lett.

Giant magnetoresistance in zigzag graphene nanoribbon

Z. F. Wang and Feng Liu[a)]

Department of Materials Science and Engineering, University of Utah, Salt Lake City, Utah 84112, USA

Based on the mean-field Hubbard model (J. Guo *et al.*, Appl. Phys. Lett. **92**, 163109 (2008)), ballistic spin transport in zigzag graphene nanoribbons is investigated theoretically. A giant magnetoresistance effect is found with 100% change in resistance as the two transverse electrodes switch from the parallel to antiparallel magnetic configuration. Such change is shown to arise from different coupling between the subbands near the Fermi level, which is dependent of the orbital symmetry. In addition, the operating energy window of giant magnetoresistance exists in a wide range of ribbon widths, easing the way for experimental validation of the proposed device. © 2011 *American Institute of Physics*. [doi:10.1063/1.3619817]

Graphene has shown many useful properties for potential applications in electronics,[1] such as extreme flexibility and stability, high carrier mobility, and long spin relaxation time. In addition, nanopatterning of graphene provides an attractive route towards large scale device integration.[2–4] In particular, graphene nanoribbons (GNRs) can be used as the device building blocks to make junctions with perfect atomic interface with a constant work function,[3] while the free edges of GNRs make them accessible to doping and chemical modification.[3,5,6] Furthermore, GNRs with zigzag edges (ZGNRs) have shown magnetism by theories due to the localized edge states,[7,8] which opens up possibilities of making graphene-based low-dimensional magnetic nanostructures[9] and potential applications of ZGNRs in spintronics.[10–12] Recently, the edge state magnetism in graphene has been indirectly confirmed in the experiment.[13]

A key concept in spintronics is the giant magnetoresistance (GMR) effect, representing the paradigm under which commercial devices such as magnetic reading heads operate nowadays. The GMR reflects the large resistance difference between two magnetic configurations. Recently, two ZGNR-based devices exhibiting GMR have been proposed. In one device, the GMR is configured with two ferromagnetic (FM) states of ZGNR electrodes in parallel vs. antiparallel alignments;[10] in the other device, it is configured between a FM and an antiferromagnetic (AFM) state of ZGNR controlled by applying an external magnetic field.[11] However, the ground state of ZGNRs is AFM, so both these GMR devices involve excitation to the higher-energy FM states. Here, we propose a different design of ZGNR GMR device that employs only the AFM ground state, so that it may consume less energy without the need of excitation to the FM states.

The basic principle of design of our proposed GMR device is illustrated in Fig. 1, and the device size is characterized by two integers: length L and width W. Two different magnetic configurations are achieved by applying local magnetic fields at the transverse electrode regions. In one configuration, magnetic fields at the two electrodes are in parallel (P configuration), so that the whole ZGNR is at the AFM ground state with the top edge in spin-up orientation and the

bottom edge in spin-down orientation. In another configuration, the magnetic field at one electrode (the right electrode) is turned into the opposite direction antiparallel with the left (AP configuration), so that the left half of ZGNR remains in the original AFM state but the right half changes into another AFM state with spins orientated in the opposite directions. Note that the left and right half are energy degenerate, hence the whole system remains overall in the AFM ground state. Consequently, the spins on the top edge change from up to down going from left to right; while the spins on the bottom edge change from down to up. Our calculations show that the resistance differs by 100% between these two magnetic configurations, manifesting a large GMR effect. This remarkable GMR effect can be linked to the unique orbital symmetry of the ZGNR subbands near the Fermi level. Also, the energy window of these subbands, within which the GMR effect occurs, displays a nonmonotonic relationship with increasing the ribbon width. In this work, we focus on the intrinsic spin transport properties of the GMR device, impurities/defects[14] and the interfacial effects of electrodes[15] are not included in our simulation.

Our device Hamiltonian is described in nearest-neighbor, tight-binding (TB), mean-field Hubbard model,[16]

$$H = \gamma \sum_{\langle i,j \rangle,\sigma} c_{i\sigma}^{+} c_{j\sigma} + U \sum_{i,\sigma} (\langle n_{i,-\sigma} \rangle - 1/2) n_{i\sigma}, \qquad (1)$$

where $c_{i\sigma}^{+}$, $c_{i\sigma}$, and $n_{i\sigma}$ are creation, annihilation, and number operators for an electron of spin σ in a π orbital centered on the ith C atom, $\gamma = -2.6$ eV is the nearest-neighbor hopping
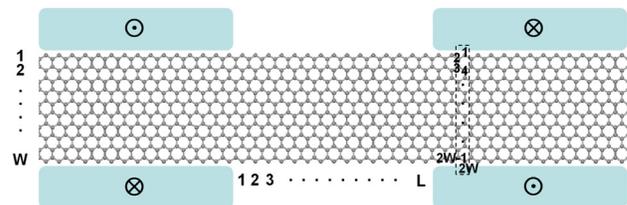
FIG. 1. (Color online) Schematic diagrams of the ZGNR GMR devices. Spin orientation of the AFM states at the transverse electrode regions is determined by the direction of the local magnetic field; $\odot$ and $\otimes$ denote the directions of local magnetic field. The width and length of the ZGNR are labeled by integer W and L, respectively.

a)Author to whom correspondence should be addressed. Electronic mail: fliu@eng.utah.edu.
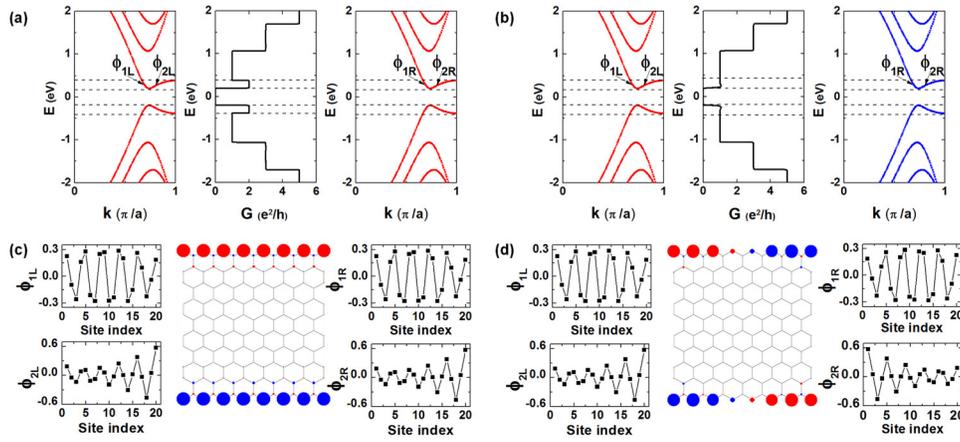
FIG. 2. (Color online) (a) and (b) are the band structures and conductance curves for the device in P and AP configurations with $W = 10$ and $L = 8$. $a = 2.46$ Å is the unit cell length along the transport direction. Left (right) panel is the band structure for left (right) lead, middle panel is the conductance curve. The dashed lines denote the energy window within which conductance dramatically changes in the P and AP configurations. The red (blue) [or light (dark)] corresponds to the spin up (down) band structure of the AFM state. (c) and (d) show the orbital (wavefunction) symmetries of the two subbands ($\phi_{1L,2L}$ for left lead and $\phi_{1R,2R}$ for right lead) within the dashed-line regions and the corresponding spin density in P and AP configurations. Left (right) panel is the wavefunction for left (right) lead, middle panel is the spin density. The site index denotes the position of the carbon atoms in the unit cell of the lead, as shown in Fig. 1. The red (blue) [or light (dark)] refers to spin up (down), the radius of the circle around each atom corresponds to the value of local spin density.

integral, and $U = 2.75$ eV is the strength of the local on-site Coulomb interaction between opposite spins. The average local spin occupancy $\langle n_{i\sigma} \rangle$ is given by

$$\langle n_{i\sigma} \rangle = -\frac{1}{\pi} \int_{-\infty}^{E_f} dE \, Im(G_{ii,\sigma}^R), \qquad (2)$$

where $E_f = 0$ is the Fermi energy, $G_\sigma^R = (E - H_\sigma - \Sigma_{l\sigma}^R - \Sigma_{r\sigma}^R)^{-1}$ is the retarded Green's function, and $\Sigma_{l\sigma/r\sigma}^R$ is the self-energy matrix of the left and right lead. Equations (1) and (2) are solved self-consistently for obtaining the converged $\langle n_{i\sigma} \rangle$ in the device region, which gives a domain wall solution for AP configuration. The spin dependent ballistic conductance of the device is calculated using the Landauer-Büttiker formalism[17]

$$G_\sigma = \frac{e^2}{h} Tr(\Gamma_{l\sigma} G_\sigma^R \Gamma_{r\sigma} G_\sigma^A), \qquad (3)$$

where $G_\sigma^A = G_\sigma^{R+}$, and $\Gamma_{\sigma/r\sigma}$ describes the coupling of the device region to left/right lead, which is given by $\Gamma_{\sigma/r\sigma} = i(\Sigma_{l\sigma/r\sigma}^R - \Sigma_{l\sigma/r\sigma}^A)$.

Figure 2 shows our numerical results for the GMR device in P and AP configurations with $W = 10$ and $L = 8$. We draw special attention to the two small energy windows, one above and one below the Fermi energy ($E_f = 0$), as marked by the dashed lines in Figs. 2(a) and 2(b). The conductance within these two energy windows is significantly different between the two configurations. In the P configuration, the conductance is $2G_0$ (Fig. 2(a), middle panel). In contrast, in the AP configuration, the conductance is quenched to $\sim G_0$ (Fig. 2(b), middle panel). Outside these two energy windows, the conductance in the P and AP configurations is the same. Since the AFM ground state of ZGNR is spin degenerated, we only show the spin up-to-up (Fig. 2(a)) and spin up-to-down (Fig. 2(b)) transport here.

We found that the change of conductance curves is closely related to the orbital symmetry of the two subbands (conducting channels) within each dashed-line energy win-

dow.[10,18,19] In the P configuration, because each edge conducts electrons of same spin (middle panel in Fig. 2(c)), the wavefunctions associated with both channels have the matching in-phase symmetry going from left to right, as shown by ϕ_{1L} vs. ϕ_{1R} and ϕ_{2L} vs. ϕ_{2R} in Fig. 2(c). Consequently, each channel contributes one G_0 conductance, amounting to a total conductance of $2G_0$. In the AP configuration, because the spin will flip direction when electrons propagate along the edges (middle panel in Fig. 2(d)), the wavefunctions associated with one channel have the matching in-phase symmetry going from left to right (Fig. 2(d), ϕ_{1L} vs. ϕ_{1R}), but those associated with the other channel have the mismatching out-of-phase symmetry (Fig. 2(d), ϕ_{2L} vs. ϕ_{2R}). Consequently, only one channel with the matching symmetry makes the major contribution to the total conductance amounting to $\sim G_0$. Outside the energy window denoted by the dashed lines, the wavefunctions of all channels have the matching symmetry in both P and AP configurations, leading to the same conductance in both configurations.

As in a standard GMR device, its efficiency is characterized by the percentage change of resistance between two magnetic configurations. Here, we produce two magnetic configurations by applying the local magnetic fields to change the direction of the AFM state in the two transverse electrode regions; similar definition of magnetoresistance (MR) can be used to describe the efficiency of our device as[10]

$$MR = \frac{R_{AP} - R_P}{R_P}, \qquad (4)$$

where $R_{P/AP} = 1/G_{P/AP}$ is the resistance in the P and AP configurations. In Fig. 3(a), we plot the MR as a function of the energy for ZGNR with $W = 10$ and $L = 8$. We see that the MR saturates to about 100% in the dashed-line region (with an energy window $\Delta = 0.18$ eV).

We have also studied the effect of ribbon size on the GMR. First, we fix the length ($L = 8$) of the device and change its width, as shown in Fig. 3(b). We found that the energy window (Δ) within which MR $\sim$ 100% displays a
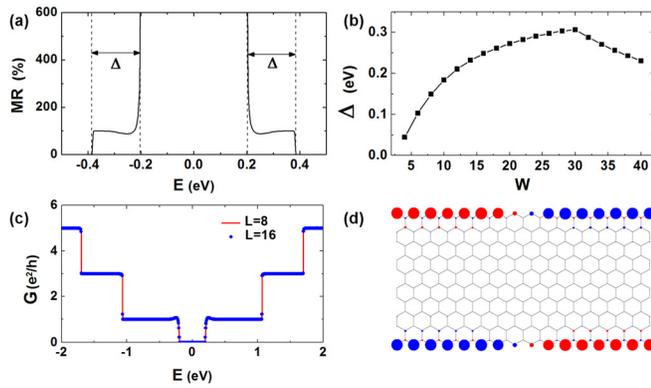
FIG. 3. (Color online) (a) MR of ZGNR device with $W = 10$ and $L = 8$. The energy window for the MR effect is bracketed by the dashed lines, $\Delta = 0.18$ eV, within which MR saturates around 100%. (b) The width of the MR energy window (Δ) as a function of ZGNR width (W) with fixed length $L = 8$. (c) Comparison of conductance in the AP configuration between two different device length $L = 8$ (solid line) and $L = 16$ (dot line) with $W = 10$. (d) Spin density distribution in the AP configuration with $W = 10$ and $L = 16$.

linear dependence on the ribbon width, first increasing then decreasing with the increasing ribbon width, and the maximum window is 0.3 eV for the ribbon width $W = 30$. The GMR energy window is defined as the energy range between the bottom of conduction band (or the top of valence band) and the band edge at $k = \pi/a$, as marked by dashed lines in Figs. 2(a) and 2(b). For the narrow ribbons ($W < 30$), the band gap decreases with the increasing ribbon width, and meantime the band edges at $k = \pi/a$ increases, leading to an increase of GMR energy window. For the wide ribbons ($W > 30$), however, some subbands begin to move into the GMR energy window originally defined by the band edges, which effectively redefines the GMR energy window to a small value. Next, we fix the width ($W = 10$) and change the length. In Fig. 3(c), we compare the conductance curves for $L = 8$ and $L = 16$ in the AP configuration. The two curves essentially overlap with each other, indicating that the GMR effect is not sensitive to the length of the device for $L \geq 8$. In our calculation, we assume that sufficiently away from the device region, the mean-field Hamiltonian of the lead is identical to that of an infinite ZGNR. This hypothesis is reasonable as long as the device region is long enough. The result in Fig. 3(c) shows that this condition is at least satisfied with $L = 8$. To see this more clearly, we plot the spin density for $L = 16$ in AP configuration in Fig. 3(d). Similar to the case for $L = 8$ in Fig. 2(d) (middle panel), a spin depletion region exists at the interface between the two AFM states of different spin orientations. The amplitude of spin density decreases rapidly at the interface region and gradually changes spin direction, which is very similar to Kim's results for antiparallel FM states.[10] The depletion region is

very narrow, spanning over four edge atoms, beyond which the spin density almost recovers to the infinite long limit. In large devices, the spin-wave-like domain walls will dominate the spin-collinear configurations considered here because of the weak magnetic anisotropy in graphene.[20]

In summary, utilizing AFM ground state of ZGNRs, we propose a mechanism for designing graphene based GMR device. Local magnetic field is used to direct the spin orientation. Resistance is found to change 100% when two transverse electrodes switch from the parallel to antiparallel magnetic configuration. This difference is revealed to arise from different coupling between the subbands near the Fermi level, which is dependent of the orbital symmetry. In addition, the GMR exists in a wide range of ZGNRs, which makes the proposed mechanism easier to be implemented in the real device.

[1]K. S. Novoselov, A. K. Geim, S. V. Morozov, D. Jiang, M. I. Katsnelson, I. V. Grigorieva, S. V. Dubonos, and A. A. Firsov, Nature **438**, 197 (2005).
[2]C. Berger, Z. Song, X. Li, X. Wu, N. Brown, C. Naud, D. Mayou, T. Li, J. Hass, A. N. Marchenkov, E. H. Conrad, P. N. First, and W. A. D. Heer, Science **312**, 1191 (2006).
[3]Q. Yan, B. Huang, J. Yu, F. Zheng, J. Zang, J. Wu, B. Gu, F. Liu, and W. Duan, Nano Lett. **7**, 1469 (2007).
[4]Z. F. Wang and F. Liu, ACS Nano **4**, 2459 (2010).
[5]Z. F. Wang, Q. Li, H. Zheng, H. Ren, H. Su, Q. W. Shi, and J. Chen, Phys. Rev. B **75**, 113406 (2007).
[6]F. Wu, E. Kan, H. Xiang, S. Wei, M. Whangbo, and J. Yang, Appl. Phys. Lett. **94**, 223105 (2009).
[7]K. Nakada, M. Fujita, G. Dresselhaus, and M. S. Dresselhaus, Phys. Rev. B **54**, 17954 (1996).
[8]Y. Miyamoto, K. Nakada, and M. Fujita, Phys. Rev. B **59**, 9858 (1999).
[9]D. Yu, E. M. Lupton, H. J. Gao, C. Zhang, and F. Liu, Nano Res. **1**, 497 (2008).
[10]W. Y. Kim and K. S. Kim, Nature Nanotechnol. **3**, 408 (2008).
[11]F. Muñz-Rojas, J. Fernández-Rossier, and J. J. Palacios, Phys. Rev. Lett. **102**, 136810 (2009).
[12]H. Santos, L. Chico, and L. Brey, Phys. Rev. Lett. **103**, 086801 (2009).
[13]C. Tao, L. Jiao, O. V. Yazyev, Y. Chen, J. Feng, X. Zhang, R. B. Capaz, J. M. Tour, A. Zettl, S. G. Louie, H. Dai, and M. F. Crommie, Nature Phys. 1991.
[14]B. Huang, F. Liu, J. Wu, B. Gu, and W. Duan, Phys. Rev. B **77**, 153411 (2008).
[15]N. Nemec, D. Tománek, and G. Cuniberti, Phys. Rev. Lett. **96**, 076802 (2006).
[16]J. Guo, D. Gunlycke, and C. T. White, Appl. Phys. Lett. **92**, 163109 (2008).
[17]S. Datta, *Electronic Transport in Mesoscopic Systems* (Cambridge University Press, New York, 1995).
[18]Z. Li, H. Qian, J. Wu, B. Gu, and W. Duan, Phys. Rev. Lett. **100**, 206802 (2008).
[19]Z. F. Wang, Q. Li, Q. W. Shi, X. Wang, J. Yang, J. G. Hou, and J. Chen, Appl. Phys. Lett. **92**, 133114 (2008).
[20]O. V. Yazyev and M. I. Katsnelson, Phys. Rev. Lett. **100**, 047209 (2008).